

The MOG weak field approximation and observational test of galaxy rotation curves

J. W. Moffat^{1,2*}, S. Rahvar^{1,3†}

¹ *Perimeter Institute for Theoretical Physics, 31 Caroline St. N., Waterloo, ON, N2L 2Y5, Canada*

² *Department of Physics and Astronomy, University of Waterloo, Waterloo, Ontario N2L 3G1, Canada*

³ *Department of Physics, Sharif University of Technology, P.O. Box 11155-9161, Tehran, Iran*

19 April 2019

ABSTRACT

As an alternative to dark matter models, MOdified Gravity (MOG) theory is a covariant modification of Einstein gravity. The theory introduces two additional scalar fields and one vector field. The aim is to explain the dynamics of astronomical systems based only on their baryonic matter. The effect of the vector field in the theory resembles a Lorentz force where each particle has a charge proportional to its inertial mass. The weak field approximation of MOG is derived by perturbing the metric and the fields around Minkowski space-time. We obtain an effective gravitational potential which yields the Newtonian attractive force plus a repulsive Yukawa force. This potential, in addition to the Newtonian gravitational constant, G_N , has two additional constant parameters α and μ . We use the THINGS catalog of galaxies and fix the two parameters α and μ of the theory to be $\alpha = 8.89 \pm 0.34$ and $\mu = 0.042 \pm 0.004 \text{ kpc}^{-1}$. We then apply the effective potential with the fixed universal parameters to the Ursa-Major catalog of galaxies and obtain good fits to galaxy rotation curve data with an average value of $\overline{\chi^2} = 1.07$. In the fitting process, only the stellar mass-to-light ratio (M/L) of the galaxies is a free parameter. As predictions of MOG, our derived M/L is shown to be correlated with the color of galaxies. We also fit the Tully-Fisher relation for galaxies. As an alternative to dark matter, introducing an effective weak field potential for MOG opens a new window to the astrophysical applications of the theory.

1 INTRODUCTION

Observations of the dynamics of galaxies as well as the dynamics of the whole universe reveal that a main part of the universe’s mass must be missing or, in modern terminology, this missing mass is made of dark matter (Bertone et al. 2005). One of the important astronomical systems which is the subject of dark matter studies is galactic scale dynamics. The observations of galaxies reveal that there is a discrepancy between the observed dynamics and the mass inferred from luminous matter (Rubin et al. 1965; Rubin et al. 1970).

An alternative approach to the problem of missing mass is to replace dark matter by a modified gravity theory. There are various approaches to modifying gravity, such as MOdified Newtonian Dynamics (MOND) or its relativistic version the so-called TeVeS theory (Milgrom 1983; Bekenstein 2004). In some modified gravity theories, the dark energy responsible for the accelerated expansion of the universe is described by a generic function of the Einstein-Hilbert action, as in $f(R)$ -gravity models (Sobouti 2007; Saffari & Rahvar 2008). Asymptotically safe quantum gravity can produce quantum corrections derived from a renormalization group calculation, which can generate galaxy rotation curves compatible with observation (Rodrigues et al. 2010). There has also been an attempt to interpret missing mass by introducing non-local gravity (Hehl & Mashhoon 2009).

The generally covariant MOdified Gravity (MOG) theory is a scalar-tensor-vector theory (STVG) (Moffat 2006). In the fol-

lowing, we will study its astrophysical applications and possible predictions (Moffat 2006). In this theory, the dynamics of a test particle are given by a modified equation of motion in which, in addition to the curvature of space-time, a massive vector field couples to the charge of a fifth force and produces a Lorentz-type force. Since the metric field is coupled to scalar fields and a massive vector field, the solution of the field equations for a point mass is different from the point mass Schwarzschild solution of General Relativity (Moffat & Toth 2009). The predictions of MOG for the rotation curves of galaxies have been compared to the data (Brownstein & Moffat 2006a; Brownstein 2009), using a static spherically symmetric point mass solution derived from the field equations. The same approach has also been applied to the dynamics of globular clusters (Moffat & Toth 2008), clusters of galaxies (Brownstein & Moffat 2006b) and the Bullet Cluster (Brownstein & Moffat 2007).

We obtain the weak field approximation of the MOG field equations by perturbing the fields around Minkowski space-time. The result for the dynamics of a test particle is that the acceleration of a particle is driven by an effective potential. This potential contains Newtonian gravity with a larger gravitational constant G_∞ and a repulsive force with a length scale μ^{-1} associated with a massive vector field. For length scales shorter than μ^{-1} , when the Yukawa exponent is of the order of unity, the repulsive force cancels the strong attractive force and we recover Newtonian gravity. On the other hand, at larger length scales the repulsive vector field

arXiv:1306.6383v2 [astro-ph.GA] 20 Aug 2013

force becomes weaker and we obtain a Newtonian potential with a larger Newtonian constant G_∞ . The advantage of the weak field approximation, in contrast to the exact spherically symmetric point particle solution of the MOG field equations, is that we can use it to describe extended objects such as galaxies and clusters of galaxies. The agreement of General Relativity with solar system data is retained by the modified acceleration law for massive test particles, derived in the weak field approximation from the MOG field equations.

In Section (2), we review the action and the field equations of MOG. In Section (3), we obtain the weak field approximation of MOG and derive an effective potential for an arbitrary distribution of matter. In Section (4), we apply the results of the weak field approximation to two classes of galaxies. For the first class, we use the THINGS¹ catalog of nearby galaxies to fix the two free parameters α and μ of the theory. Then we apply the effective potential predictions to fit the observed galaxy rotation curves in the Ursa-Major catalog of galaxies with the only free parameter, the stellar mass-to-light ratio M/L . The M/L used to fit the galaxy data are shown to be correlated with the colors of galaxies. Based on the dynamics of galaxies derived from MOG and the luminosities of galaxies obtained from observation, we obtain results in good agreement with the Tully-Fisher relation. Section (5) contains a summary of our results.

2 FIELD EQUATIONS IN MOG

We use the metric signature convention $(+, -, -, -)$. The generic form of the MOG action is given by (Moffat 2006):

$$S = S_G + S_\phi + S_S + S_M. \quad (1)$$

It is composed of the Einstein gravity action:

$$S_G = -\frac{1}{16\pi} \int \frac{1}{G} (R + 2\Lambda) \sqrt{-g} d^4x, \quad (2)$$

the massive vector field ϕ_μ action:

$$S_\phi = -\frac{1}{4\pi} \int \omega \left[\frac{1}{4} B^{\mu\nu} B_{\mu\nu} - \frac{1}{2} \mu^2 \phi_\mu \phi^\mu + V_\phi(\phi_\mu \phi^\mu) \right] \sqrt{-g} d^4x, \quad (3)$$

and the action for the scalar fields:

$$S_S = - \int \frac{1}{G} \left[\frac{1}{2} g^{\alpha\beta} \left(\frac{\nabla_\alpha G \nabla_\beta G}{G^2} + \frac{\nabla_\alpha \mu \nabla_\beta \mu}{\mu^2} \right) + \frac{V_G(G)}{G^2} + \frac{V_\mu(\mu)}{\mu^2} \right] \sqrt{-g} d^4x. \quad (4)$$

Here, ∇_ν is the covariant derivative with respect to the metric $g_{\mu\nu}$, the Faraday tensor of the vector field is defined by $B_{\mu\nu} = \partial_\mu \phi_\nu - \partial_\nu \phi_\mu$, ω is a dimensionless coupling constant, G is a scalar field representing the gravitational coupling strength and μ is a scalar field corresponding to the mass of the vector field. Moreover, $V_\phi(\phi_\mu \phi^\mu)$, $V_G(G)$ and $V_\mu(\mu)$ are the self-interaction potentials associated with the vector field and the scalar fields, respectively. The action for pressureless dust can be written as

$$S_M = \int (-\rho \sqrt{u^\mu u_\mu} - \omega Q_5 u^\mu \phi_\mu) \sqrt{-g} d^4x. \quad (5)$$

Here, ρ is the density of matter and Q_5 is the fifth force source charge, which is related to the mass density, $Q_5 = \kappa \rho$, where κ is a constant.

Varying the action with respect to the fields results in the MOG field equations. We start by varying the matter action S_M with respect to the metric, which yields the energy-momentum tensor:

$$T_{\mu\nu} = -\frac{2}{\sqrt{-g}} \frac{\delta(S_M + S_\phi + S_S)}{\delta g^{\mu\nu}}. \quad (6)$$

The variation of S_M with respect to the vector field ϕ_μ results in the fifth force current:

$$J^\mu = -\frac{1}{\sqrt{-g}} \frac{\delta S_M}{\delta \phi_\mu}. \quad (7)$$

For the dynamics of a test particle, we adopt the action of a point particle (Moffat 2006; Moffat & Toth 2009) which can also be obtained by substituting $\rho(x) = m\delta^3(x)$ in equation (5):

$$S_{tp} = \int (-m - \omega q_5 \phi_\mu u^\mu) d\tau. \quad (8)$$

Here q_5 is the fifth force charge of the test particle, which is related to the inertial mass of the particle, $q_5 = \kappa m$. Varying this action results in the equation of motion of a test particle with an extra force on the right-hand side:

$$\frac{du^\mu}{d\tau} + \Gamma^\mu_{\alpha\beta} u^\alpha u^\beta = \omega \kappa B^\mu_{\alpha} u^\alpha. \quad (9)$$

As in General Relativity, the equation of motion is independent of the mass of the test particle, so that the particle motion satisfies the weak equivalence principle. A main difference between this equation of motion and the standard geodesic equation in General Relativity is that the fifth force contributes an extra repulsive force which depends on the velocity of the particle. We set for simplicity the potentials of the fields to zero i.e., $V_\phi(\phi_\mu \phi^\mu) = V(G) = V(\mu) = 0$.

3 WEAK FIELD APPROXIMATION IN MOG

As we noted in the introduction, the exact static spherically symmetric solution of the MOG field equations has been obtained for a point-like mass (Moffat & Toth 2009). For extended physical systems, we must use numerical calculations to solve the nonlinear MOG field equations.

A natural way to study the behaviour of MOG on astrophysical scales is to derive a weak field approximation for the dynamics of the fields. Our aim is to obtain the field equations for such a weak field approximation by perturbing the fields around Minkowski space-time for an arbitrary distribution of non-relativistic matter.

We perform a perturbation of the metric around the Minkowski metric $\eta_{\mu\nu}$:

$$g_{\mu\nu} = \eta_{\mu\nu} + h_{\mu\nu}. \quad (10)$$

For the vector field, we have

$$\phi_\mu = \phi_{\mu(0)} + \phi_{\mu(1)}, \quad (11)$$

where $\phi_{\mu(0)}$ is the zeroth order and $\phi_{\mu(1)}$ the first order perturbations. For Minkowski space-time, we set $\phi_{\mu(0)}$ equal to zero, for in the absence of matter there is no gravity source for the vector field ϕ_μ . We write for convenience $\phi_{\mu(1)} = \phi_\mu$. For the scalar field G , we perturb it around the Minkowski metric background:

$$G = G_{(0)} + G_{(1)}, \quad (12)$$

¹ <http://www.mpia-hd.mpg.de/THINGS/Overview.html>

where $G_{(0)}$ is a constant in Minkowski space. We perturb the scalar field μ around the Minkowski space background:

$$\mu = \mu_{(0)} + \mu_{(1)}, \quad (13)$$

where $\mu_{(0)}$ is a constant which we for convenience will label as μ . We assume that $\mu_{(1)}$ is negligibly small and fix the scalar field μ in equation (4) to be the constant value μ , representing the mass of the vector field. Finally, we perturb the energy-momentum tensor about the Minkowski background:

$$T_{\mu\nu} = T_{\mu\nu(0)} + T_{\mu\nu(1)}. \quad (14)$$

We vary the action with respect to the three fields $g_{\mu\nu}$, G and ϕ_μ , taking into account the perturbations around flat space. Varying the action with respect to the G field gives

$$\square G_{(1)} = -\frac{G_{(0)}}{16\pi} R_{(1)}, \quad (15)$$

where $R_{(1)}$ is the first order perturbation of the Ricci scalar. Again, for convenience, we replace the background value of $G_{(0)}$ by G_0 .

Varying the action with respect to the metric and ignoring the higher orders of perturbation, we get

$$R_{\mu\nu(1)} - \frac{1}{2} R_{(1)} \eta_{\mu\nu} = -8\pi G_0 T_{\mu\nu(1)}^{(M)} - 8\pi G_0 T_{\mu\nu(1)}^{(\phi)}, \quad (16)$$

where the first term on the right-hand side of this equation represents the energy-momentum tensor of matter, and the second term corresponds to the energy-momentum tensor of the vector field given by

$$\begin{aligned} T_{\mu\nu}^{(\phi)} &= \frac{\omega}{4\pi} (B_\mu^\alpha B_{\nu\alpha} - \frac{1}{4} g_{\mu\nu} B^{\alpha\beta} B_{\alpha\beta}) \\ &- \frac{\mu^2 \omega}{4\pi} (\phi_\mu \phi_\nu - \frac{1}{2} \phi_\alpha \phi^\alpha g_{\mu\nu}). \end{aligned} \quad (17)$$

By taking the trace of equation (16), we obtain on the left-hand side of the equation $-R_{(1)}$ and on the right-hand side the trace of the energy-momentum tensor of matter and the vector field. We will ignore the higher order perturbation of the vector field ϕ_μ , and ignore the density of the vector field compared to the density of matter (i.e., $T_{\mu\nu(1)}^{(\phi)} \ll T_{\mu\nu(1)}^{(M)}$). The trace of equation (16) can be written as

$$R_{(1)} = 8\pi G_0 T_{\mu(1)}^{\mu(M)}, \quad (18)$$

where on the right-hand side we have for pressureless matter $T_{\mu(1)}^{\mu(M)} = \rho$. Substituting equation (18) into equation (15), for the static solution, we get

$$\vec{\nabla}^2 \left(\frac{G_{(1)}}{G_0} \right) = \frac{1}{2} G_0 \rho. \quad (19)$$

From the solution of this equation, we know that $G_{(1)}/G_0$ is of the order of the gravitational potential or $(v/c)^2$ where v is the internal velocity of the system. Hence, for systems such as galaxies or clusters of galaxies, the deviation from the constant G_0 is of order $G_1/G_0 \simeq 10^{-7} - 10^{-5}$. In what follows, we only keep the background value of G_0 in our equations.

In the weak field approximation, for the (0, 0) component we have

$$R_{00(1)} = \frac{1}{2} \vec{\nabla}^2 h_{00}, \quad (20)$$

and we obtain the field equation:

$$\frac{1}{2} \vec{\nabla}^2 (h_{00}) = -4\pi G_0 \rho. \quad (21)$$

For the vector field, we obtain the field equation by varying the action with respect to ϕ^μ :

$$\nabla_\nu B^{\mu\nu} - \mu^2 \phi^\mu = -\frac{4\pi}{\omega} J^\mu. \quad (22)$$

Let us assume that the vector matter current J^μ is conserved, $\nabla_\mu J^\mu = 0$, then we can impose in the weak field approximation the gauge condition, $\phi^\mu_{,\mu} = 0$. For the static case, we obtain

$$\vec{\nabla}^2 \phi^0 - \mu^2 \phi^0 = -\frac{4\pi}{\omega} J^0, \quad (23)$$

which has the solution

$$\phi^0(x) = \frac{1}{\omega} \int \frac{e^{-\mu|\vec{x}-\vec{x}'|}}{|\vec{x}-\vec{x}'|} J^0(\vec{x}') d^3 x'. \quad (24)$$

In order to obtain the field equation for an effective potential in the weak field approximation, we take the divergence of the spatial component of the equation of motion (9):

$$\vec{\nabla} \cdot \vec{a} - \frac{1}{2} \vec{\nabla}^2 h_{00} = -\omega \kappa \vec{\nabla}^2 \phi^0, \quad (25)$$

where \vec{a} represents the acceleration of the test particle. We substitute $\vec{\nabla}^2 h_{00}$ from (21) into (25) and relate directly the acceleration of the test particle to the distribution of matter. We define the effective potential for the test particle by, $\vec{a} = -\vec{\nabla} \Phi_{eff}$, and relate it to the distribution of matter:

$$\vec{\nabla} \cdot (\vec{\nabla} \Phi_{eff} - \kappa \omega \vec{\nabla} \phi^0) = 4\pi G_0 \rho. \quad (26)$$

On the left-hand side of this equation, we define Φ_N as the solution to the Poisson equation:

$$\Phi_N = \Phi_{eff} - \kappa \omega \phi^0. \quad (27)$$

Substituting the solution for ϕ^0 from (24) by replacing J^0 with $\kappa \omega \rho$, and using the solution of Φ_N from equation (27), the effective potential becomes

$$\Phi_{eff}(\vec{x}) = - \int \frac{G_0 \rho(\vec{x}')}{|\vec{x}-\vec{x}'|} d^3 x' + \kappa^2 \int \frac{e^{-\mu|\vec{x}-\vec{x}'|}}{|\vec{x}-\vec{x}'|} \rho(\vec{x}') d^3 x'. \quad (28)$$

Here, the first term corresponds to the attractive gravitational force, while the second term is the repulsive Yukawa force. For a point mass particle, using the Dirac-delta function $\rho(\vec{x}') = M \delta^3(\vec{x}')$, the effective potential reduces to

$$\Phi_{eff}(x) = -\frac{G_0 M}{x} + \kappa^2 \frac{M e^{-\mu x}}{x}, \quad (29)$$

where $x = |\vec{x}|$. For small distances compared to μ^{-1} , we can expand the exponential term yielding the effective potential:

$$\Phi_{eff}(x) = -\frac{(G_0 - \kappa^2) M}{x} - \mu \kappa^2 M. \quad (30)$$

The constant second term on the right-hand side does not enter into the dynamics of the test particle; the first term should be the Newtonian gravitational contribution and we obtain

$$G_0 - \kappa^2 = G_N.$$

On the other hand, at large distances (i.e. $\mu x \rightarrow \infty$), we just have the first term of equation (29). Hereafter, we rename G_0 as G_∞ which corresponds to the effective gravitational constant at infinity.

Substituting G_0 and κ^2 into (28), the effective potential for an extended distribution of matter in MOG in the weak field approximation is given by

$$\Phi_{eff}(\vec{x}) = -G_\infty \left[\int \frac{\rho(\vec{x}')}{|\vec{x}-\vec{x}'|} \left(1 - \frac{G_\infty - G_N}{G_\infty} e^{-\mu|\vec{x}-\vec{x}'|} \right) d^3 x' \right]. \quad (31)$$

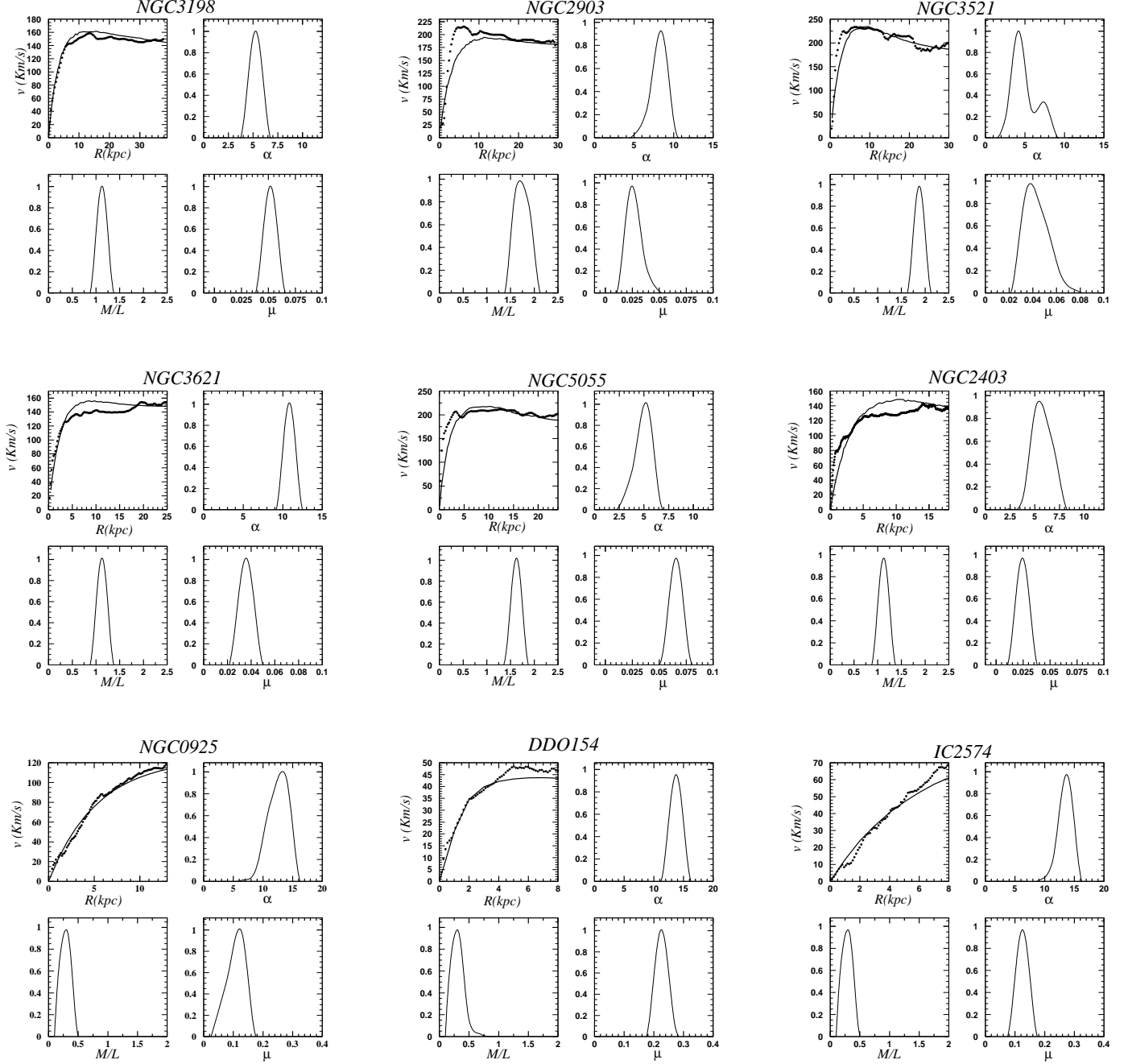


Figure 1. The best fit for the sub-sample of THINGS galaxies with the corresponding marginalized likelihood functions of α , μ and M/L . Here in this list we have both HBS and LSB galaxies. Table (1) provides the best values of the parameters with the corresponding error bars.

Now we use the same notation as used by Moffat and Toth (2009), defining $\alpha = (G_\infty - G_N)/G_N$. Then the effective potential can be written as

$$\Phi_{eff}(\vec{x}) = -G_N \left[\int \frac{\rho(\vec{x}')}{|\vec{x} - \vec{x}'|} (1 + \alpha - \alpha e^{-\mu|\vec{x} - \vec{x}'|}) d^3x' \right], \quad (32)$$

and the acceleration of the test particle can be obtained from the

gradient of the potential, $\vec{a} = -\vec{\nabla}\Phi_{eff}$, yielding the result

$$\begin{aligned} \vec{a}(\vec{x}) &= -G_N \int \frac{\rho(\vec{x}')(\vec{x} - \vec{x}')}{|\vec{x} - \vec{x}'|^3} [1 + \alpha \\ &\quad - \alpha e^{-\mu|\vec{x} - \vec{x}'|} (1 + \mu|\vec{x} - \vec{x}'|)] d^3x'. \end{aligned} \quad (33)$$

In the weak field approximation, we shall treat α and μ as constant parameters. However, in the exact static spherically symmetry solution μ and α depend on the mass of the source (Moffat & Toth 2009). In the weak approximation limit, any

deviation from Newtonian gravity depends on the size of the system.

In the next section, by means of a numerical calculation of the potential for spiral galaxies, we compare the weak field approximation limit of MOG to observational data for the rotation curves of galaxies.

4 ROTATION CURVES OF SPIRAL GALAXIES

In this section, we investigate the rotation curves of spiral galaxies determined by the distribution of baryonic matter, which is made of stars and interstellar gas without exotic dark matter. For a galaxy with cylindrical symmetry, the radial component of acceleration can be calculated by discretizing space into small elements and adding the acceleration of each element as follows

$$a_r(r) = G_N \sum_{r'=0}^{\infty} \sum_{\theta'=0}^{2\pi} \frac{\Sigma(r')}{|r-r'|^3} (-r+r'\cos\theta')(1+\alpha -\alpha e^{-\mu|r-r'|} - \mu\alpha|r-r'|e^{-\mu|r-r'|})r'\Delta r'\Delta\theta', \quad (34)$$

where $\Sigma(r)$ represents the column density of a spiral galaxy.

From the observations, we have the column density of stars in a given color band as well as the column density of hydrogen. Fitting the distribution of matter with an exponential function, we can identify any spiral galaxy with the following parameters, (i) the total luminosity of the galaxy in a given filter (here we will use data from the B-band and the infrared band), (ii) the total hydrogen of the galaxy from 21cm observations and, (iii) the characteristic length scale of the galaxy R , which is the length scale occurring in the exponential law for the column density of a galaxy (Fathi et al. 2010):

$$\Sigma(r) = \Sigma_0 \exp(-r/R). \quad (35)$$

Integrating over the surface to infinity, the total mass of the disk is related to R and the central column density, $M_{disk} = 2\pi\Sigma_0R^2$. Thus, knowing M_{disk} and R , we can calculate Σ_0 . For the gaseous component of the galaxy, we obtain the mass of gas from Hydrogen and Helium abundance from Big Bang nucleosynthesis, $M_{gas} = (4/3)M_H$. In the calculation of the mass of the stars, we assume a stellar mass-to-light ratio, Υ_* , and the total mass of the stars can be obtained from $M_{stars} = \Upsilon_* \times L$, where L is the overall luminosity of the galaxy in a given filter.

We choose a sub-sample of nearby galaxies, the THINGS catalog with high resolution measurements of velocity and density of hydrogen profile (de Blok et al. 2008). For this set of galaxies, we adopt in the weak field approximation μ and α as well as the stellar mass-to-light ratio M/L when fitting the rotation curves of galaxies to the data. We then find the best values of α and μ and fix these two parameters. Then we fit the observed rotation curves of the larger Ursa-Major sample of galaxies, letting the stellar mass-to-light ratio M/L be the only free parameter.

4.1 THINGS catalog

The HI Nearby Galaxy Survey (THINGS) catalog contains nearby galaxies with high resolution observations of rotation velocities and distributions of matter. These observations provide high quality HI rotation curves together with the column density of hydrogen (de Blok et al. 2008; Walter et al. 2008; Leroy et al. 2008). Here, we also use stellar distributions for this sample of galaxies and the $3.6\mu\text{m}$ band images from SINGS (Kennicutt et al 2003).

From the color of stars in each part of a galaxy, we can measure the mass of the stellar components of the disk obtained from the correlation between the color and the stellar mass-to-light ratio (Oh et al. 2008). We also use Near Infra Red (NIR) information in addition to the shorter wavelengths such as B band, for which the mass-to-light ratio is mainly dominated by the young stellar population. We note that NIR mainly probes the old stellar populations (Bell & de Jong 2001).

The THINGS catalog contains 19 galaxies, but we choose a sub-sample of 9 galaxies, which have full coverage of rotation curves from the centre to the edges of the galaxies. Table (1) shows the list of galaxies in the sub-sample of the THINGS catalog. As we noted before, we let the parameters of the effective potential and the stellar mass-to-light ratio ($M/L = \Upsilon_*$) change during the fitting of the theoretical rotation curves to the galaxy data. Figure (1) shows the best fit to the data with the corresponding marginalized likelihood functions for the three free parameters of the model. The best values for the modified gravity parameters α and μ , with the corresponding mass-to-light ratios M/L , are given in Table (1).

In order to calculate an average value for α and μ , we use the combined likelihood functions of nine different galaxies in the THINGS catalog. Since the data for the galaxies are independent, the overall likelihood function is the multiplication of each of the distributions, $P = \prod_{i=1}^9 P_i$. Hence for our set of galaxies the overall likelihood function can be written as

$$P(\chi^2) \propto \exp\left(-\frac{1}{2} \sum_{i=1}^9 [\chi^2 - \chi_i^2(\text{min})]\right). \quad (36)$$

From the combined likelihood functions, we obtain the best fit parameters of MOG: $\alpha = 8.89 \pm 0.34$ and $\mu = 0.042 \pm 0.004 \text{ kpc}^{-1}$.

4.2 Ursa-Major Galaxies

We adopt the best fit values of α and μ , obtained from the THINGS galaxies fitting process, as universal parameters and let the stellar mass-to-light ratio Υ_* of the galaxies be the only free parameter. We find the best value of Υ_* by fitting the observed rotation curves of galaxies with MOG. Figure (2) represents the observational data with the best fits to the rotation curves of the galaxies. Table (2) lists the galaxies with the best stellar mass-to-the light ratio and the best χ^2 per degree of freedom for each galaxy. We have used in the fits to the observed data R , L_B and M_H (Verheijen & Sancisi 2001a ; Verheijen & Sancisi 2001b; Tully et al. 1996) given in Table (2). In this list of results, we have three outliers: NGC3972 with $\chi^2 = 3.43$, NGC4389 with $\chi^2 = 2.59$ and UGC6930 with $\chi^2 = 2.20$. For the rest of the galaxies, we have very good results for the fitting of the data with the average value of χ^2 for all the galaxies $\overline{\chi^2} = 1.07$. We also use again the THINGS catalog and let only the mass-to-light ratio of stars M/L be the free parameter. The best fits to the light curves are shown in Figure (3). The best value for $\Upsilon_*^{3.6}$ with the associated value of χ^2 is shown in Table (3).

4.3 Stellar mass-to-light ratio and color of galaxies

In star formation scenarios, the stellar mass-to-light ratio is related to the color of galaxies (Bell & de Jong 2001; Bell et al. 2003). This relation depends on the details of the history of star formation and the initial mass function (IMF). However, there are a number of uncertainties due to the Stellar Population Synthesis (SPS) models and the choice of IMF. Also due to dust in the interstellar medium

Table 1. The sub-sample of galaxies from the THINGS catalog with the best fit parameters obtained from fitting the observed rotation curves to the MOG theoretical rotational curves. The description of the columns is given by, (1) the name of the galaxy, (2) type of galaxy, (3) distances of the galaxies, (4) the overall luminosity of the galaxies in the B-band, (5) the characteristic size of the galaxy in eq. (35), (6) the overall hydrogen mass of the galaxy, (7) the overall mass of the galaxy calculated by $M_{disk} = \frac{4}{3}M_{HI} + L_B \times \Upsilon_*$, (8) the best fit value of α , (9) the best fit value of μ and, (10) the stellar mass-to-light ratio for each galaxy. The error bars are obtained from the likelihood functions given in Figure (1). Observational data are taken from the THINGS publications in (de Blok et al. 2008; Walter et al. 2008; Leroy et al. 2008).

Galaxy (1)	Type (2)	Distance (Mpc) (3)	L_B ($10^{10} L_B$) (4)	R_0 (kpc) (5)	M_{HI} ($10^{10} M_\odot$) (6)	M_{disk} ($10^{10} M_\odot$) (7)	α (8)	μ (kpc^{-1}) (9)	Υ_* (M_\odot/L_\odot) (10)
NGC 3198	HSB	13.8	3.241	4.0	1.06	4.72	5.94 ± 1.01	0.051 ± 0.012	1.02 ± 0.13
NGC 2903	HSB	8.9	4.088	3.0	0.49	7.35	8.02 ± 1.78	0.032 ± 0.007	1.64 ± 0.14
NGC 3521	HSB	10.7	4.769	3.3	1.03	6.23	4.31 ± 1.03	0.037 ± 0.013	1.02 ± 0.06
NGC 3621	HSB	6.6	2.048	2.9	0.89	3.48	9.82 ± 0.31	0.027 ± 0.011	1.12 ± 0.08
NGC 5055	HSB	10.1	3.622	2.9	0.76	6.59	5.40 ± 0.060	0.057 ± 0.006	1.54 ± 0.16
NGC 2403	LSB	3.2	1.647	2.7	0.46	2.45	5.60 ± 0.61	0.018 ± 0.007	1.12 ± 0.13
DDO 0154	LSB	4.3	0.007	0.8	0.03	0.04	13.71 ± 1.23	0.22 ± 0.03	0.29 ± 0.1
IC 2574	LSB	4.0	0.345	4.2	0.19	0.35	13.70 ± 1.30	0.12 ± 0.028	0.3 ± 0.2
NGC 0925	LSB	9.2	1.444	3.9	0.41	0.95	13.10 ± 1.7	0.11 ± 0.03	0.28 ± 0.11

Table 2. HSB and LSB galaxies from the set of Ursa-Major galaxies (Verheijen & Sancisi 2001a ; Verheijen & Sancisi 2001b; Tully et al. 1996). The columns are depicted as follows: (1) name of the galaxy, (2) type of galaxy, (3) distance of the galaxy from us, (4) the luminosity of the galaxy in the B-filter, (5) the characteristic length of the galaxy, (6) mass of hydrogen, (7) the overall mass of the galaxy calculated by $M_{disk} = \frac{4}{3}M_{HI} + L_B \times \Upsilon_*$, (8) the reddening-corrected color (Sanders & Verheijen 1998), (9) internal extinction of galaxy in the B band, (10) the best fit for the stellar mass-to-light ratio Υ_* , normalized to the solar value and, (11) the normalized χ^2 for the best fit to the data.

Galaxy (1)	Type (2)	Distance (Mpc) (3)	L_B ($10^{10} L_B$) (4)	R_0 (kpc) (5)	M_{HI} ($10^{10} M_\odot$) (6)	M_{disk} ($10^{10} M_\odot$) (7)	B-V (mag) (8)	A_B (mag) (9)	Υ_* M_\odot/L_\odot (10)	χ^2 $1/N.d.f$ (11)
NGC 3726	HSB	17.4	3.340	3.2	0.60	4.00	0.45	0.06	$0.96^{+0.06}_{-0.06}$	1.66
NGC 3769	HSB	15.5	0.684	1.5	0.41	1.87	0.64	0.084	$1.94^{+0.18}_{-0.18}$	1.60
NGC 3877	HSB	15.5	1.948	2.4	0.11	3.92	0.68	0.084	$1.94^{+0.12}_{-0.12}$	0.22
NGC 3893	HSB	18.1	2.928	2.4	0.59	5.09	0.56	0.077	$1.47^{+0.12}_{-0.12}$	0.96
NGC 3917	LSB	16.9	1.334	2.8	0.17	2.57	0.60	0.077	$1.76^{+0.09}_{-0.09}$	1.75
NGC 3949	HSB	18.4	2.327	1.7	0.35	2.93	0.39	0.078	$1.06^{+0.07}_{-0.07}$	0.63
NGC 3953	HSB	18.7	4.236	3.9	0.31	8.97	0.71	0.109	$2.02^{+0.08}_{-0.08}$	1.63
NGC 3972	HSB	18.6	0.978	2.0	0.13	1.89	0.55	0.051	$1.76^{+0.12}_{-0.12}$	3.43
NGC 4010	LSB	18.4	0.883	3.4	0.29	2.45	–	0.088	$2.34^{+0.22}_{-0.22}$	0.8
NGC 4013	HSB	18.6	2.088	2.1	0.32	5.14	0.83	0.060	$2.26^{+0.06}_{-0.06}$	1.18
NGC 4051	HSB	14.6	2.281	2.3	0.18	3.45	0.62	0.047	$1.41^{+0.12}_{-0.12}$	1.59
NGC 4085	HSB	19.0	1.212	1.6	0.15	1.75	0.47	0.066	$1.28^{+0.18}_{-0.18}$	0.79
NGC 4088	HSB	15.8	2.957	2.8	0.64	4.66	0.51	0.071	$1.29^{+0.09}_{-0.09}$	0.59
NGC 4100	HSB	21.4	3.388	2.9	0.44	5.19	0.63	0.084	$1.36^{+0.05}_{-0.05}$	1.75
NGC 4138	LSB	15.6	0.827	1.2	0.11	3.45	0.81	0.051	$4.00^{+0.47}_{-0.47}$	0.10
NGC 4157	HSB	18.7	2.901	2.6	0.88	5.64	0.66	0.077	$1.54^{+0.10}_{-0.10}$	0.16
NGC 4183	HSB	16.7	1.042	2.9	0.30	1.92	0.39	0.055	$1.46^{+0.11}_{-0.11}$	0.25
NGC 4217	HSB	19.6	3.031	3.1	0.30	5.55	0.77	0.063	$1.70^{+0.07}_{-0.07}$	0.46
NGC 4389	HSB	15.5	0.610	1.2	0.04	0.73	–	0.053	$1.12^{+0.23}_{-0.23}$	2.59
UGC 6399	LSB	18.7	0.291	2.4	0.07	1.03	–	0.061	$3.24^{+0.32}_{-0.32}$	0.29
UGC 6446	LSB	15.9	0.263	1.9	0.24	0.72	0.39	0.059	$1.54^{+0.19}_{-0.19}$	1.46
UGC 6667	LSB	19.8	0.422	3.1	0.10	1.14	0.65	0.058	$2.40^{+0.20}_{-0.20}$	0.05
UGC 6917	LSB	18.9	0.563	2.9	0.22	1.70	0.53	0.098	$2.52^{+0.18}_{-0.18}$	0.34
UGC 6923	LSB	18.0	0.297	1.5	0.08	0.61	0.42	0.096	$1.70^{+0.24}_{-0.24}$	0.85
UGC 6930	LSB	17.0	0.601	2.2	0.29	1.51	0.59	0.108	$1.88^{+0.15}_{-0.15}$	2.20
UGC 6983	LSB	20.2	0.577	2.9	0.37	1.72	0.45	0.096	$2.14^{+0.20}_{-0.20}$	0.44
UGC 7089	LSB	13.9	0.352	2.3	0.07	0.69	–	0.055	$1.70^{+0.21}_{-0.21}$	0.35

of galaxies, we may observe galaxies redder and fainter than their actual color and magnitude.

For the Salpeter mass function (Salpeter 1995), the relation between the mass-to-light ratio Υ_*^B in the B band and for the color of galaxies is given by (Bell et al. 2003):

$$\log(\Upsilon_*^B) = 1.74(B - V) - 0.94. \quad (37)$$

Using Kroupa's IMF, the slope of this function does not change. However in equation (37) the mass-to-light ratio shifts by the amount -0.35 dex.

The relation between the mass-to-light ratios and the color of

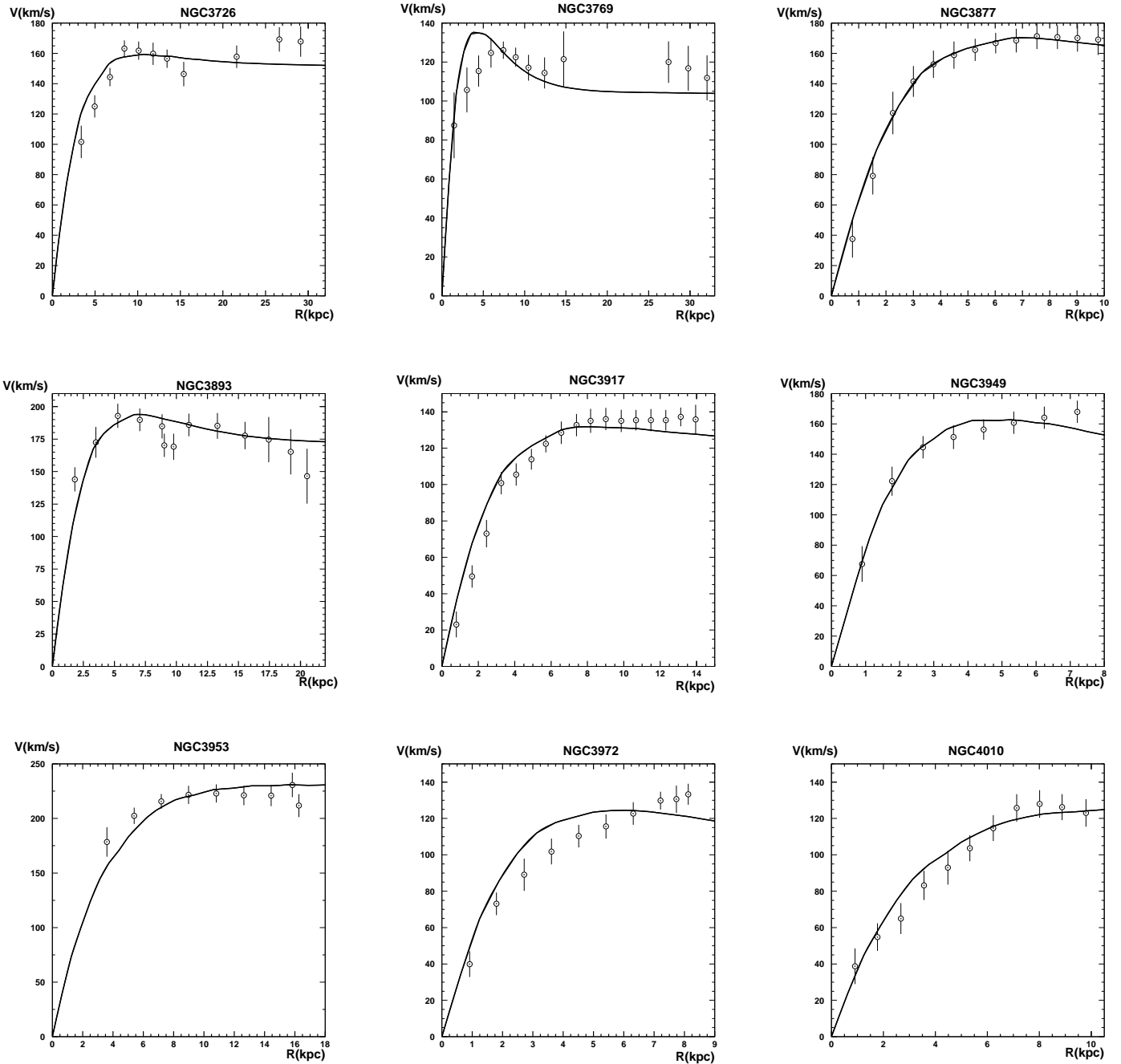


Figure 2. The best fit to the rotation velocity curves of the Ursa-Major sample. We fix $\alpha = 8.89$ and $\mu = 0.042 \text{ kpc}^{-1}$ from the fits to the THINGS catalog. We take the stellar mass-to-light ratio Υ_* as the free degree of freedom.

galaxies has been investigated in the longer wavelengths. The advantage of longer wavelength is that the uncertainty in this relation dramatically decreases near the infrared (NIR). Here we adopt the results of the analysis of the magnitudes of galaxies in the J, H and K bands (Bell & de Jong 2001) as well as the observations in the $3.6\mu\text{m}$ band. From the SPS models the relation between the mass-to-light ratio in the K band and the color in the J-K band is given by (Bell & de Jong 2001):

$$\log(\Upsilon_*^K) = 1.43(J - K) - 1.38. \quad (38)$$

On the other hand, from the relation between Υ_*^K and $\Upsilon_*^{3.6}$ (Oh et al. 2008):

$$\Upsilon_*^{3.6} = 0.92\Upsilon_*^K - 0.05, \quad (39)$$

we can relate $\Upsilon_*^{3.6}$ to the J-K band. Again for the case of Kroupa's IMF, we decrease the constant term in equation (38) by the amount 0.15.

Finally, in order to compare the mass-to-light ratio derived from MOG with the stellar synthesis models, we plot in Figure (4) the mass-to-light ratio both for the Ursa-Major galaxies in the B

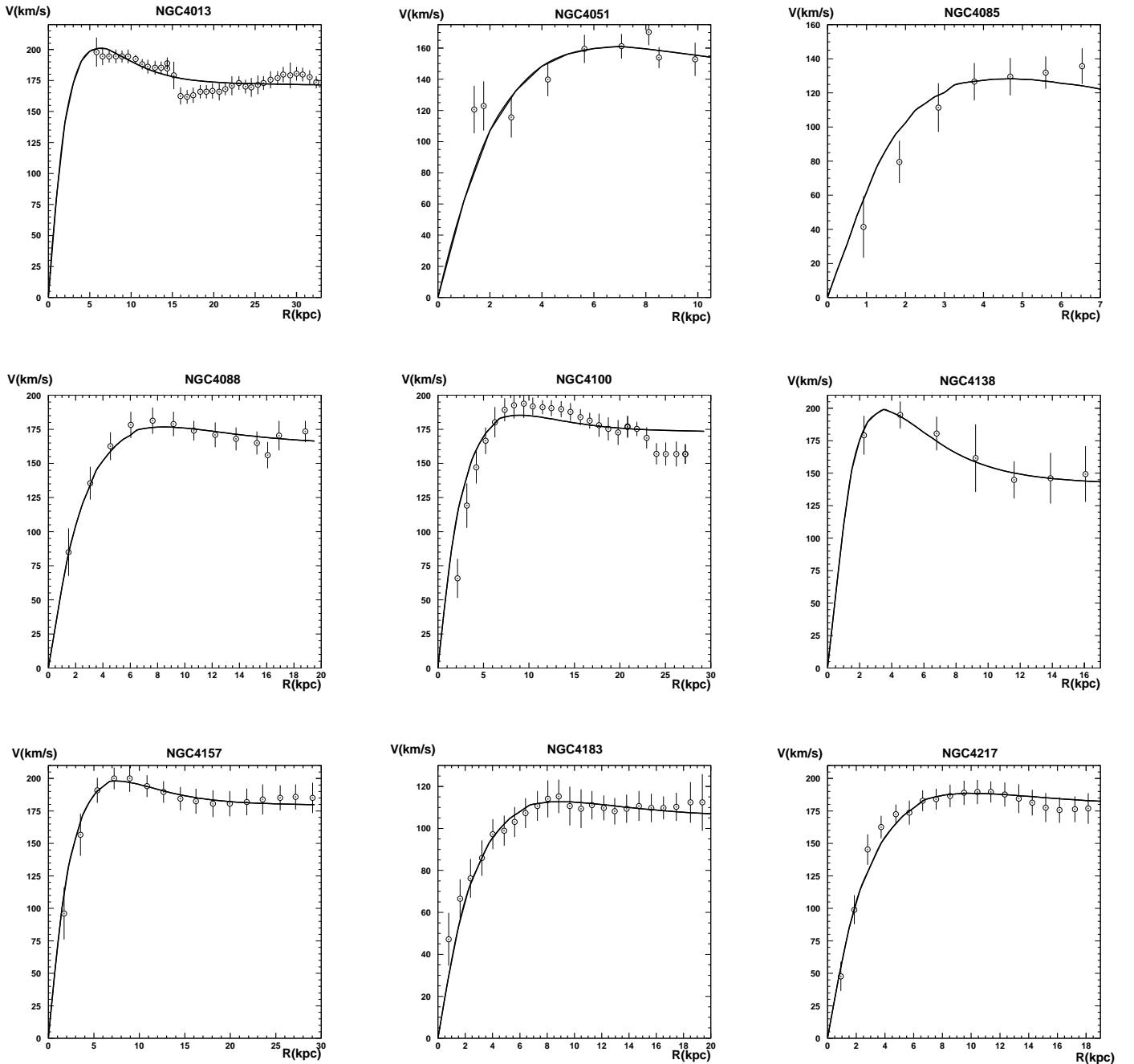


Figure 2. –continued

band and the THINGS catalog in the $3.6\mu\text{m}$ band and compare the result with equations (37) and (38). We note that the colors and the magnitudes of galaxies in the Ursa-Major galaxies are extinction corrected. Also in order to study the behaviour of galaxies based on their types, we divide galaxies in this plot into two class of HSB and LSB galaxies. For the LSB galaxies we have larger values of mass-to-light ratios compared to the HSB galaxies. This effect also has been reported by fitting rotation curves of galaxies with a dark matter model (Verheijen & Tully 1999). The differences between the mass-to-light ratios for the HSB and LSB galaxies has been

studied in (Zwaan et al. 1995), where for the the LSB galaxies Υ_* is twice as big for the HSB galaxies.

While the physical correlation between Υ_* and the color of galaxies has been proved, there are still uncertainties in the analytical relation between these two parameters. One of the uncertainties in equation (38) is the initial mass function (IMF) of the stars. Bell & de Jong (2010) showed that to have stellar disks consistent with the dynamics, the so-called “diet” Salpeter IMF has to have the stars’ masses reduced below $0.35M_{\odot}$. Relation (38) corresponds to the diet Salpeter IMF. In this case, the stellar mass has to be

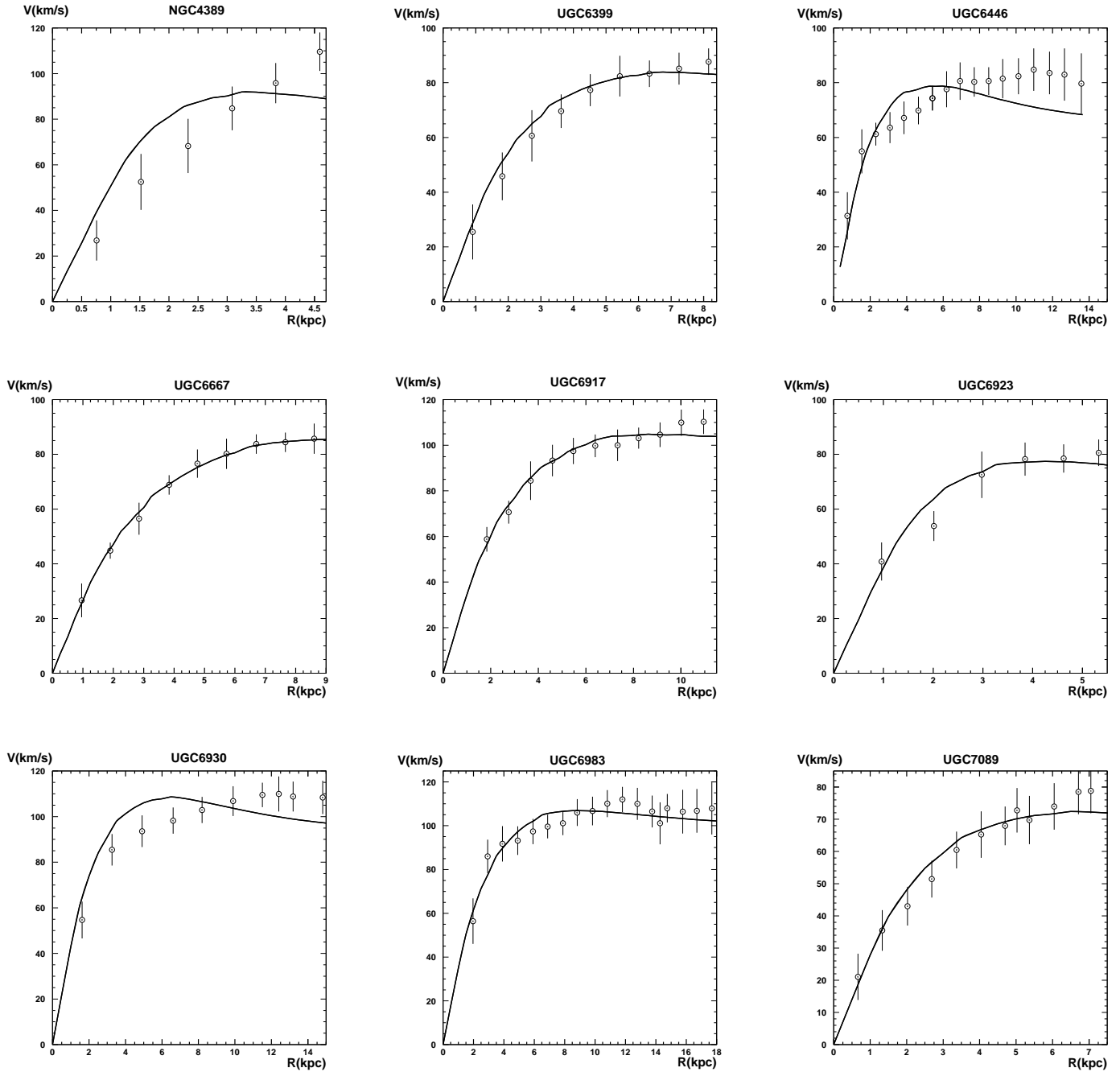


Figure 2. –continued

reduced by a factor of 0.7. Moreover, near infrared observations provide more reliable values for the stellar mass-to-light ratio than the visual band observations. In Figure (4), the stellar mass-to-light ratio obtained from MOG in the $3.6\mu\text{m}$ band is more compatible with the theoretical model. By dividing Υ_* for the LSB galaxies by 2, we get results compatible with the theoretical model.

4.4 Tully-Fisher Relation

Observations by Tully and Fisher (1977) showed that there is an empirical relation between rotation curves of galaxies and their luminosities, $v_c^4 \propto L$. We want to test whether this relation is satisfied in MOG. The right-hand side of the Tully-Fisher relation (absolute magnitude) can be obtained from observations, using the apparent magnitude, distance and extinction factor. On the other hand, the rotation curves of galaxies, as we discussed in the pervious sections, are measured. Here we adopt the rotation velocities of galaxies from the best fits of MOG to the data, given in the last sections.

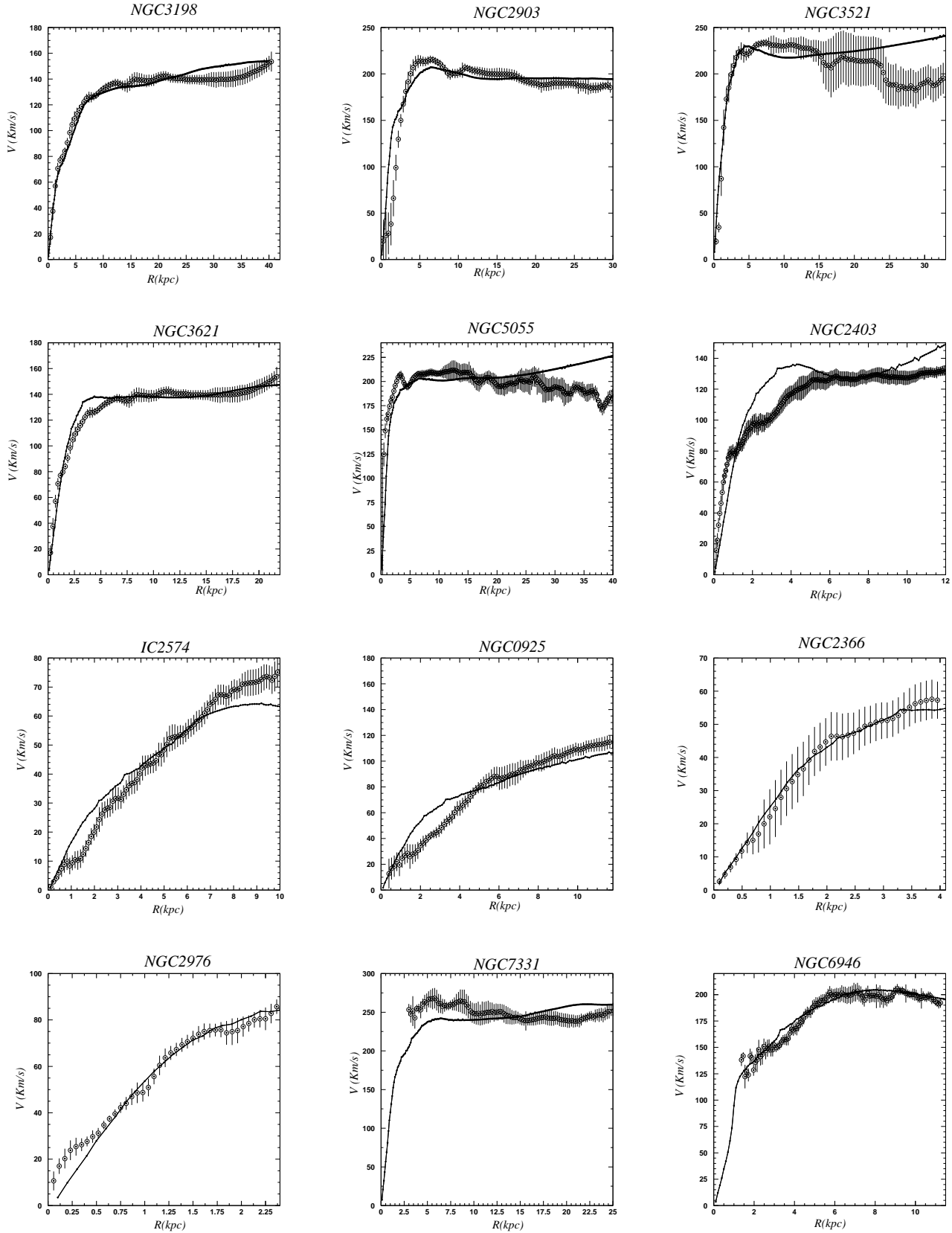


Figure 3. The best fit to the rotation velocity curves of the THINGS sample. We fix $\alpha = 8.89$ and $\mu = 0.042 \text{ kpc}^{-1}$ and let the stellar mass-to-light ratio $\Upsilon_{\star}^{3.6}$ be the only free parameter.

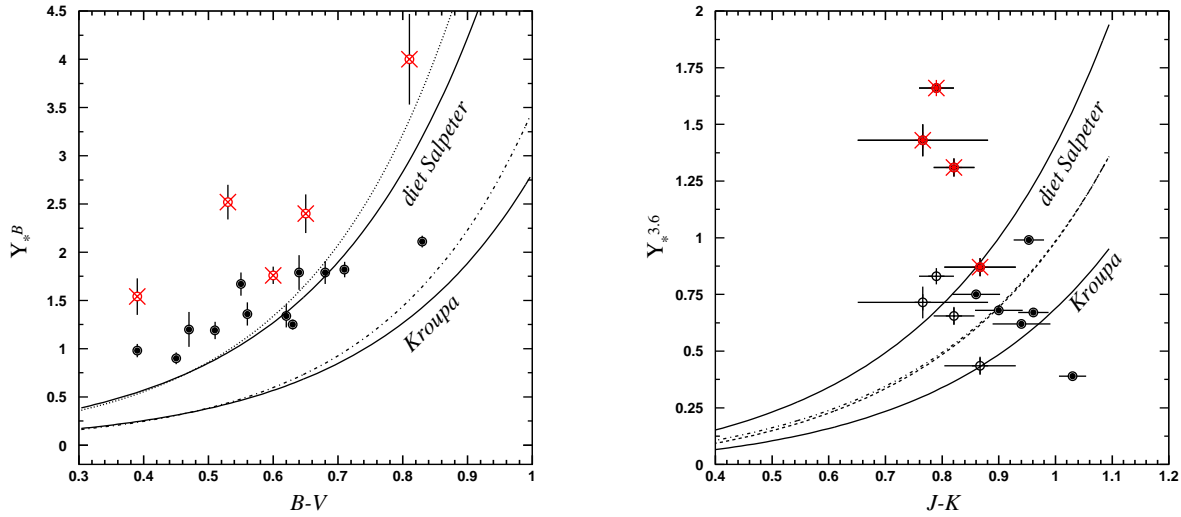


Figure 4. Stellar mass-to-light ratio as a function of color of the galaxies in the Ursa-Major catalog (left panel) and the galaxies in the THINGS catalog (right panel). For the Ursa-Major galaxies, Υ_* is given in the B band, while for the THINGS galaxies it is in the $3.6\mu\text{m}$ band. The theoretical models for both the “diet” Salpeter and Kroupa IMF models are depicted as solid lines with the margins to the models shown as dotted lines in both panels. The black dots in both panels represent HSB galaxies, while the red color cross signs represent LSB galaxies. In the right panel, we have normalized Υ_* by a factor of 2 for the LSB galaxies represented by open circles.

Table 3. Results obtained from fitting galaxies in the THINGS catalog with the MOG rotation curves for the case of the fixed parameters $\alpha = 0.89$ and $\mu = 0.042 \text{ kpc}^{-1}$. The columns of this table are as follows: (1) name of the galaxy, (2) the type of galaxy, (3) distance of the galaxy, (4) color of the galaxy in the $(J - k)$ band (Jarrett et al. 2003), (5) the stellar mass-to-light ratio $\Upsilon_*^{3.6}$ in the $3.6\mu\text{m}$ band, derived from MOG, (6) the reduced χ^2 .

Galaxy (1)	Type (2)	Distance (Mpc) (3)	$J - K$ (4)	$\Upsilon_*^{3.6}(\text{MOG})$ (M_\odot/L_\odot) (5)	$\chi^2/N_{d.o.f}$ (6)
NGC 3198	HSB	13.8	0.940 ± 0.051	0.63 ± 0.01	1.24
NGC 2903	HSB	8.9	0.915 ± 0.024	2.37 ± 0.03	2.10
NGC 3521	HSB	10.7	0.953 ± 0.027	0.99 ± 0.02	3.02
NGC 3621	HSB	6.6	0.860 ± 0.042	0.76 ± 0.01	1.64
NGC 5055	HSB	10.1	0.961 ± 0.027	0.67 ± 0.01	4.28
NGC 2403	LSB	3.2	0.790 ± 0.031	1.68 ± 0.01	7.78
IC 2574	LSB	4.0	0.766 ± 0.115	1.43 ± 0.07	2.24
NGC 0925	LSB	9.2	0.867 ± 0.063	0.87 ± 0.04	3.67
NGC 2366	LSB	3.4	0.667 ± 0.146	2.76 ± 0.23	0.08
NGC 2976	LSB	3.6	0.821 ± 0.036	1.31 ± 0.04	1.43
NGC 7331	HSB	14.7	1.03 ± 0.024	0.39 ± 0.01	4.11
NGC 6946	HSB	5.9	0.90 ± 0.042	0.68 ± 0.01	1.20

For the the Tully-Fisher relation, we can use both the maximum rotation curve of the galaxies, V_{max} , and the flat rotation curve, V_{flat} .

In order to calculate the flat rotation curve, we adopt the convention in (Verheijen 2001): (a) for the galaxies with a rising rotation curve, V_{flat} cannot be measured, (b) for the galaxies with a flat rotation curve, $V_{flat} = V_{max}$, (c) for galaxies with a declining rotation curve V_{flat} is calculated from averaging the outer parts of the galaxy. Figure (5) displays the distribution of galaxies in terms of apparent magnitude versus the logarithm of the flat rotation curve. The best fit to the data is given by the apparent magnitude:

$$M_b = -8.27 \times \log_{10}(V_{flat}) - 1.99. \quad (40)$$

The slope of this function is compatible with the observational data

analyzed by Verheijen (2001). For various samples of galaxies the slope of the observed data in equation (40) changes from -8.7 ± 0.3 to -9.0 ± 0.4 .

5 CONCLUSIONS

We have developed the weak field approximation of MOG as an alternative to dark matter models. MOG is a covariant modified gravity theory which contains tensor, vector and scalar fields in the action. The non-linear field equations in MOG and the equation of motion for a massive test particle were applied to the study of the dynamics of galaxies. The modified equation of motion contains an extra contribution from the gradient of the vector field ϕ_μ , propor-

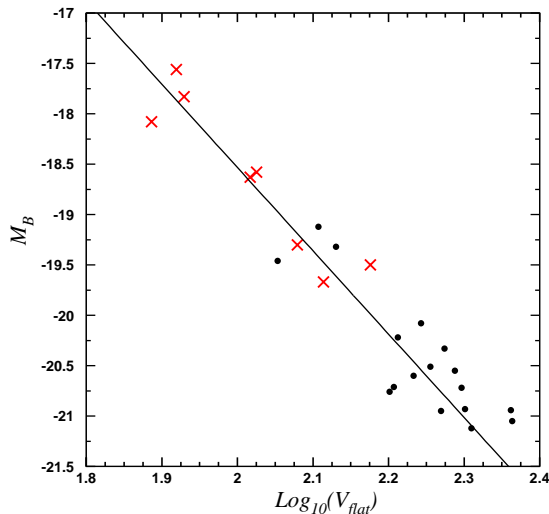


Figure 5. The absolute magnitude of galaxies in the Ursa-Major catalog as a function of the logarithm of the flat rotation curve. The linear relation is the Tully-Fisher relation. The black spots represent the HSB galaxies and the red cross signs represent the LSB galaxies. The flat rotation curves in this figure are taken from the MOG fits to the data. The best fit to the data is obtained for $M = -8.27 \times \log(V_{flat}) - 1.99$.

tional to the fifth force charge q_5 , which is related to the inertial mass, $q_5 = \kappa m$.

We expanded the fields in the MOG action around Minkowski space-time and combined the test particle equation of motion with the field equations. An effective potential for an arbitrary distribution of matter was obtained. For any extended object this effective potential is composed of an attractive and a repulsive Yukawa contribution. It contains two free parameters α and μ , where $1/\mu$ is the characteristic length scale associated with the vector field ϕ_μ . We have shown that the effective potential at small and large scales is given by the Newtonian potential, but with different effective gravitational constants.

To test the observational consequences of the effective potential, we used the well measured THINGS catalog of galaxies to fit the theoretical rotation curves predicted by MOG to the observed data. This catalog of galaxies contains both LSB and HSB galaxies. For this set of galaxies, we let the three parameters of the model, α , μ and the stellar mass-to-light ratio, Υ_* be the free parameters of the theory. The best values from the combined likelihood functions yielded $\alpha = 8.89 \pm 0.34$ and $\mu = 0.042 \pm 0.004 \text{ kpc}^{-1}$. As for the second step, we used a larger set of Ursa-Major galaxies and with the fixed universal parameters $\alpha = 8.89 \pm 0.34$ and $\mu = 0.042 \pm 0.004 \text{ kpc}^{-1}$, we let the mass-to-light ratio Υ_* of the galaxies be the only free parameter in the fitting of the data. We obtained excellent fits for the velocity rotation curves to the observational data with the average value $\chi^2/N_{dof} = 1.07$.

As a prediction of MOG, we compared the deduced stellar mass-to-light ratios of galaxies with their colors both for the THINGS and the Ursa-Major galaxies. Depending on the Initial Mass Function (IMF) the theoretical relation between these two parameters can change. In addition there is more uncertainty in the shorter wavelengths data compared to the Near Infrared wavelengths data. Our MOG prediction in the infrared wavelengths

($3.6\mu\text{m}$) was consistent with the predictions of theoretical astrophysical models. The advantage of this result is that, knowing the color of galaxies in the infrared ($J - K$), we obtain valuable information about the stellar mass to light ratios M/L . On the other hand, from the luminosity of galaxies in the visual band and the HI radio emission data, we can obtain the baryonic masses of the galaxies. From this information, we are able to calculate the dynamics of galaxies and other large-scale systems, such as clusters of galaxies and the merging of galaxies *without any free parameters*. This means that there will be no free degrees of freedom in MOG when calculating the dynamics of astrophysical systems.

In dark matter models in which galaxies are fitted with a dark matter spherical halo, it has not been possible so far to obtain parameter-free fits to rotation velocity curve data. Dark matter profiles require at least two free parameters for each galaxy, in addition to the stellar mass-to-light ratio, to enable fits to rotation curve data. This is in contrast to our results for MOG which yields excellent fits to rotation curve data with only one free parameter, M/L .

Moreover, we can successfully predict the Tully-Fisher relation for galaxies because of the direct relationship between rotation curves and luminous matter. This is not possible in standard dark matter models because there is no relation between the dominant dark matter and the stellar luminosity of galaxies. We used the values of the flat rotation curves of galaxies predicted by MOG and plotted the absolute magnitudes of the galaxies in terms of $\log(V_{flat})$. The best fit to the data has a slope of -8.27 , which is in good agreement with the observed data. Our analysis from the solar system scale to the galactic scales showed that MOG is a consistent covariant modified gravity theory without exotic dark matter, and for these scales we can replace the non-linear MOG field equations with an effective weak field gravitational potential, which can be easily adapted to any astrophysical system.

ACKNOWLEDGMENTS

The John Templeton Foundation is thanked for its generous support of this research. The research was also supported by the Perimeter Institute for Theoretical Physics. The Perimeter Institute was supported by the Government of Canada through Industry Canada and by the Province of Ontario through the Ministry of Economic Development and Innovation. We also would like to thank Niayesh Afshordi, Viktor Toth and Martin Green for helpful discussions and comments.

REFERENCES

- Bell, E. F., & de Jong, R. S. 2001, ApJ, 550, 212
- Bell E. F., McIntosh D. H., Katz N., Weinberg M. D., 2003, ApJS, 149, 289
- Bekenstein, J. D. 2004, Phys Rev D, 70, 083509
- Bertone, G., Hooper, D., & Silk, J. 2005, Physics Report, 405, 279
- de Blok, W. J. G., Walter, F., Brinks, E., et al. 2008, AJ, 136, 2648
- Brownstein, J. R., & Moffat, J. W. 2006, ApJ, 636, 721
- Brownstein, J. R., & Moffat, J. W. 2006, Mon. Not. Roy. Astron. Soc. 367, 527
- Brownstein, J. R., & Moffat, J. W. 2007, Mon. Not. Roy. Astron. Soc. 382, 29
- Brownstein, J. R. 2009, Ph.D. Thesis, University of Waterloo.
- Fathi, K., Allen, M., Boch, T., Hatziminaoglou, E., & Peletier, R. F. 2010, MNRAS, 406, 1595

- Hehl, F. W., & Mashhoon, B. 2009, *Physics Letters B*, 673, 279
- Jarrett, T. H., Chester, T., Cutri, R., Schneider, S., & Huchra, J. P. 2003, *AJ*, 125, 525
- Kennicutt, R. C., Jr., et al. 2003, *PASP*, 115, 928
- Leroy, A. K., Walter, F., Brinks, E., et al. 2008, *AJ*, 136, 2782
- Hehl, F. W., & Mashhoon, B. 2009, *Physics Letters B*, 673, 279
- Milgrom, M. 1983, *ApJ*, 270, 365
- Moffat, J. W., 2006, *JCAP*, 3, 4
- Moffat, J. W., Toth, V. T. 2008, *ApJ*, 680, 1158
- Moffat, J. W., Toth, V. T., 2009, *Classical and Quantum Gravity* 26 (8), 085002
- Oh, S.-H., de Blok, W. J. G., Walter, F., Brinks, E., & Kennicutt, R. C., Jr. 2008, *AJ*, 136, 2761
- Rubin, V. C., Burbidge, E. M., Burbidge, G. R., & Prendergast, K. H. 1965, *ApJ*, 141, 885
- Rodrigues, D. C., Letelier, P. S., & Shapiro, I. L. 2010, *JCAP*, 4, 20
- Rubin V. C. & Ford, W. K., Jr. 1970, *ApJ*, 159, 379
- Saffari, R., & Rahvar, S. 2008, *Phys Rev D*, 77, 104028
- Salpeter E. E., 1955, *ApJ*, 121, 161
- Sanders, R. H., & Verheijen, M. A. W. 1998, *ApJ*, 503, 97
- Sobouti, Y. 2007, *A&A*, 464, 921
- Tully, R. B., & Fisher, J. R. 1977, *A&A*, 54, 661
- Tully, R. B., Verheijen, M. A. W., Pierce, M. J., Huang, J.-S., & Wainscoat, R. J. 1996, *AJ*, 112, 2471
- Verheijen, M. A. W. 2001, *ApJ*, 563, 694
- Verheijen, M., & Tully, B. 1999, *The Low Surface Brightness Universe*, 170, 92
- Verheijen, M. A. W., & Sancisi, R. 2001, *A&A*, 370, 765
- Verheijen, M. A. W., & Sancisi, R. 2001, *VizieR Online Data Catalog*, 337, 765
- Walter, F., Brinks, E., de Blok, W. J. G., Bigiel, F., Kennicutt, R. C., Thornley, M. D and Leroy, A., 2008, *AJ* 136, 2563
- Zwaan, M. A., van der Hulst, J. M., de Blok, W. J. G., & McGaugh, S. S. 1995, *MNRAS*, 273, L35